Functional photoacoustic microscopy of pH

M. Rameez Chatni, Junjie Yao, Amos Danielli, Christopher P. Favazza, Konstantin I. Maslov, et al.

M. Rameez Chatni, Junjie Yao, Amos Danielli, Christopher P. Favazza, Konstantin I. Maslov, Lihong V. Wang, "Functional photoacoustic microscopy of pH," Proc. SPIE 8223, Photons Plus Ultrasound: Imaging and Sensing 2012, 82230N (23 February 2012); doi: 10.1117/12.907685

SPIE.

Event: SPIE BiOS, 2012, San Francisco, California, United States

Functional Photoacoustic Microscopy of pH

M. Rameez Chatni[a], Junjie Yao[a], Amos Danielli[a], Christopher P. Favazza[a], Konstantin I. Maslov[a], Lihong V. Wang[a]
[a] Optical Imaging Laboratory, Department of Biomedical Engineering, Washington University in St. Louis, One Brookings Drive, St. Louis, MO USA 63130

ABSTRACT

pH is a tightly regulated indicator of metabolic activity. In mammalian systems, imbalance of pH regulation may result from or result in serious illness. Even though the regulation system of pH is very robust, tissue pH can be altered in many diseases such as cancer, osteoporosis and diabetes mellitus. Traditional high-resolution optical imaging techniques, such as confocal microscopy, routinely image pH in cells and tissues using pH sensitive fluorescent dyes, which change their fluorescence properties with the surrounding pH. Since strong optical scattering in biological tissue blurs images at greater depths, high-resolution pH imaging is limited to penetration depths of 1mm. Here, we report photoacoustic microscopy (PAM) of commercially available pH-sensitive fluorescent dye in tissue phantoms. Using both optical-resolution photoacoustic microscopy (OR-PAM), and acoustic resolution photoacoustic microscopy (AR-PAM), we explored the possibility of recovering the pH values in tissue phantoms. In this paper, we demonstrate that PAM was capable of recovering pH values up to a depth of 2 mm, greater than possible with other forms of optical microscopy.

Keywords: Photoacoustic imaging, pH, optical imaging, quantitative photoacoustics, photoacoustic sensing

1. INTRODUCTION

In most mammalian systems, end-products of metabolic activity are acids. Anaerobic metabolism produces lactic acid, and aerobic metabolism produces CO_2, which is then rapidly converted to carbonic acid. The production of acid drives the tight regulation of intra-cellular and extra-cellular pH. This regulation involves the efflux of H^+ from cells and then diffusion of these H^+ into blood. pH regulation provides distinct environmental conditions for metabolic pathways, and for energy storage in the form of electrochemical potential gradients in cells. Additionally, almost all proteins depend on pH to maintain their structure and function. Even though the regulation system of pH is very robust, it can be altered in many diseases, such as cancer, osteoporosis and diabetes mellitus [1]. Since pH is a metabolic indicator, its accurate measurement can be helpful for diagnostics and therapeutics.

Traditional high-resolution optical imaging techniques, such as confocal microscopy, routinely image pH in cells and tissues by using fluorescent pH-sensitive dyes, which change their fluorescence properties with the surrounding. However, high-resolution pH images are limited to penetration depths of less than 100 μm, because strong optical scattering in biological tissue blurs the image at greater depths [2].

Photoacoustic (PA) sensing of pH has been reported previously in pH sensitive polymeric membranes using single optical wavelength approach [3]. Then an improvement on this method was demonstrated using PA ratiometric approach [7] for sensing pH in aqueous solutions of pH sensitive fluorescence dye (SNARF-5F) in clear medium. In this report, for the first time, we demonstrate PA imaging of pH in tissue phantoms, and the possibility of recovering absolute values of pH from PA signals using linear spectral unmixing at tissue depth of up to 2 mm.

Photoacoustic microscopy (PAM), an emerging biomedical imaging modality for non-invasive *in vivo* studies, has advanced tremendously since its inception [4,5]. In PAM, non-ionizing short laser pulses are delivered into biological tissue. The optical energy is partially absorbed and converted into heat. The heat causes transient thermoelastic expansion, resulting in wideband ultrasound waves which are then detected by an ultrasonic transducer placed outside the tissue [6]. With 100% sensitivity to absorption, PAM can utilize endogenous absorbers such as hemoglobin to produce high-resolution images *in vivo*. Taking advantage of non-radiation optical contrast and low ultrasonic tissue scattering, PAM holds the potential to image pH distribution *in vivo* with high sensitivity and spatial resolution.

Photons Plus Ultrasound: Imaging and Sensing 2012, edited by Alexander A. Oraevsky, Lihong V. Wang,
Proc. of SPIE Vol. 8223, 82230N · © 2012 SPIE · CCC code: 1605-7422/12/$18 · doi: 10.1117/12.907685

Based on the focus mechanisms, PAM has two different implementations. For optical-resolution photoacoustic microscope (OR-PAM), its lateral resolution (~5 μm) is derived from tight optical focusing by an objective with NA of 0.1 [7]. Its axial resolution (~15 μm) is determined by time-resolved acoustic detection, and penetration depth (~700 μm) is similar to other high-resolution optical microscopy techniques [7]. OR-PAM relies on ballistic photons and obeys the penetration limit of one transport mean free path.

For acoustic-resolution photoacoustic microscope (AR-PAM) [4,5], the fiber-guided laser beam is passed through a conical lens to form a ring-shaped illumination (dark-field), and then focused with the ultrasonic transducer. Because the optical focus is much wider than the acoustic focus, AR-PAM spatial resolutions are mostly determined by the acoustic parameters. Since ultrasound scattering is 2-3 orders weaker than optical scattering in biological tissue, an axial resolution of 15 μm and lateral resolution of 45 μm have been achieved with a maximum penetration depth of ~3 mm *in vivo*[5]. Unlike OR-PAM and other optical microscopy techniques, AR-PAM does not rely on ballistic photons. It can provide speckle-free high-resolution structural, functional, and molecular imaging at depths greater than one transport mean free path in biological tissue. However, in order to further scale the lateral resolution to less than 5 microns, the acoustic frequency has to be increased to more than 300 MHz. This would result in the penetration depth less than 100 μm *in vivo*[7], which is much less than OR-PAM. Therefore, working in different spatial scales, OR-PAM and AR-PAM provide complementary imaging capabilities and can meet the need of various biomedical studies.

2. METHODS

2.1 SNARF-5F buffer solutions

SNARF-5F carboxylic acid stock solution (2.12 mM) was prepared by dissolving 1 mg of SNARF-5F lyophilized powder (Invitrogen, USA) in 1 ml of 50 mM sodium phosphate buffer (pH 6.0). The SNARF-5F stock solution was then diluted to 0.1 mM using sodium phosphate buffers with pH values of 6.78, 7.45 and 7.80, and the final pH values of these diluted SNARF-5F solutions were measured by a commercial pH meter (Thermo Scientific, FL, USA).

2.2 OR-PAM imaging

For OR-PAM imaging, the phantom was prepared by injecting approximately 80 μL of each of the three 0.1 mM SNARF-5F solutions into different Silastic ® tube (Dow Corning, USA. Inner diameter: 0.3 mm; outer diameter: 0.64 mm). The phantom was loaded onto the OR-PAM scanning stage, and a 2 mm x 3 mm area was raster scanned at optical wavelengths of 565 and 580 nm. The laser repetition rate was set to 1 kHz, and pulse energy was between 60 and 80 nano-joules for OR-PAM. The PA signal was calibrated by the reference photodiode signal. To simulate the optical properties of biological tissue, freshly excised nude mouse skin tissue was overlaid on the tubes and the same imaging procedure was repeated over approximately the same area.

2.3 AR-PAM imaging

An acrylic phantom with four wells (diameter: 3 mm; center to center distance: 4.5 mm) was machined for AR-PAM imaging. The left two wells were filled with pH 7.80 SNARF-5F solution, the upper right well was filled with pH 7.45 SNARF-5F solution, and the lower right well was filled with pH 6.8 SNARF-5F solution respectively. The phantom was loaded on the AR-PAM stage, and an 11 mm × 13 mm area was raster scanned at optical wavelengths of 565 and 580 nm. The laser repetition rate was set to 1 kHz, and the pulse energy was between 230 and 300 nano-joules for AR-PAM. The PA signal was calibrated by the reference photodiode signal. Similar to the OR-PAM experiment, freshly excised chicken breast tissue was overlaid on the phantom and the same imaging procedure was repeated over approximately the same area.

3. RESULTS

3.1 SNARF-5F pH dependent absorption characteristics

Between pH 6.0 and 9.0, the SNARF-5F carboxylic acid exists as two distinct populations of acidic and basic forms that have different absorption spectra (figure 1). To determine wavelength dependent molar extinction coefficients of both the acidic and basic forms, 20 μM of SNARF-5F buffer solutions were prepared at pH 4.0 and 10.0 respectively. Then the

absorption spectra of both forms were measured using Cary 5000 UV-Vis absorption spectrometer (Varian, USA). From the absorbance measurements, the molar extinction coefficients were determined for both forms of SNARF-5F dye shown in figure 1.

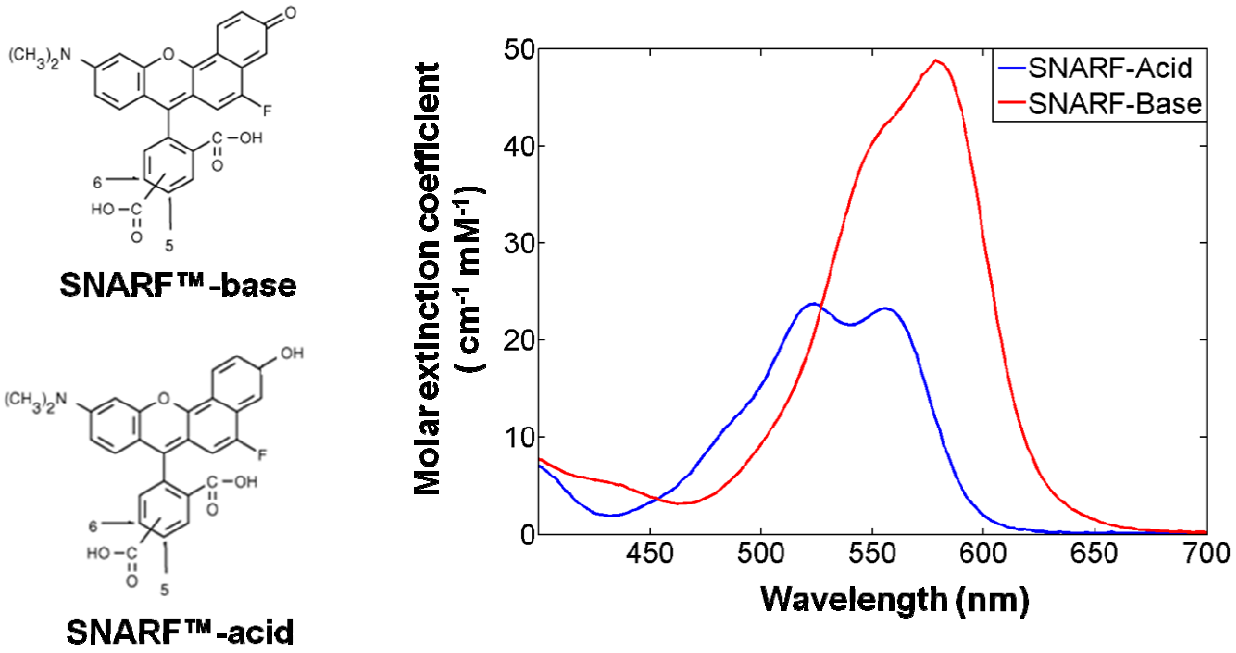

Figure 1. Absorption spectra of acidic and basic forms of SNARF-5F.

3.2 pH sensing in phantoms

Since SNARF-5F exists as acidic and basic forms with distinct absorption spectra, linear spectral unmixing was utilized to calculate the relative concentrations of acid and base species. Then the ratio of these concentrations was calculated to determine the pH from the Handersson-Hasselbach equation.

To investigate the capability of photoacoustics to recover pH, 50 µL of 0.1 mM SNARF-5F buffer solutions at different pH were injected in Silastic® tubes. The tubes were scanned using the OR-PAM systems at 565 and 580 nm optical wavelengths. Twenty A-lines were averaged over the area of interest, and the amplitude of the photoacoustic signal was determined for each wavelength (figure 2). Each A-line was compensated for pulse by pulse laser energy variation. The acidic and basic concentrations of SNARF-5F were determined by solving equations (1) using linear least squares.

$$\begin{aligned} PA(\lambda_1) &= \varepsilon_{base}(\lambda_1)C_{base} + \varepsilon_{acid}(\lambda_1)C_{acid} \\ PA(\lambda_2) &= \varepsilon_{base}(\lambda_2)C_{base} + \varepsilon_{acid}(\lambda_2)C_{acid} \end{aligned} \tag{1}$$

where PA(λ) is the fluence compensated photoacoustic signal, ε_{base} and ε_{acid} are the wavelength dependent molar extinction coefficients of acid and base forms of SNARF-5F, C_{base} and C_{acid} are the relative concentrations of these acid and base forms.

Then the pH was determined using the Handersson-Hasselbach relationship in equation (2);

$$pH = pKa + \log\frac{C_{base}}{C_{acid}} \tag{2}$$

where pKa for SNARF-5F was determined to be 7.32 from absorbance measurements at 565 and 580 nm.

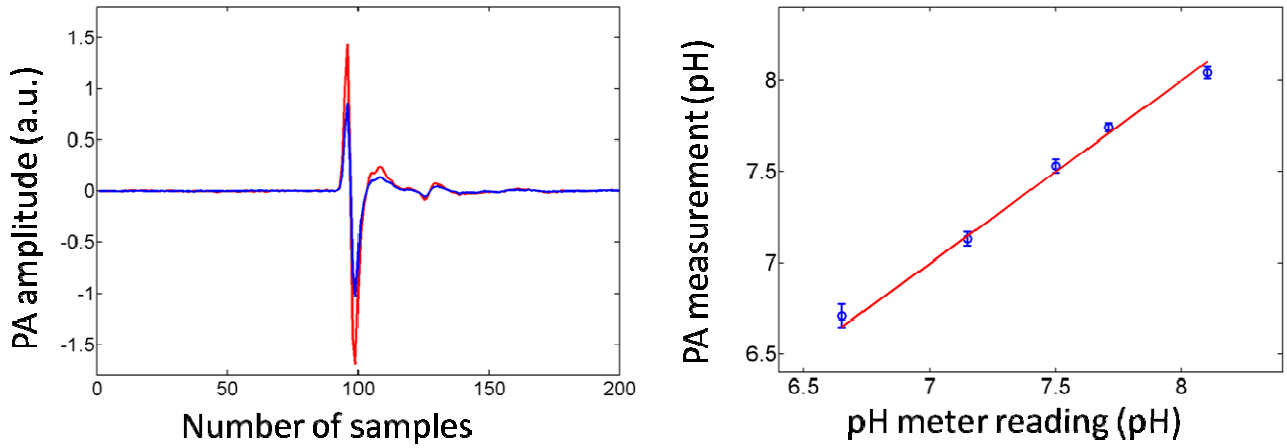

Figure 2. Comparison of pH determined by OR-PAM versus by that of determined by pH meter.

The pH measured from OR-PAM measurements were repeated 6 times at each pH and the mean and standard deviations were plotted versus the pH measured from the pH meter of the same SNARF-5F buffer solutions. The recovered pH from the photoacoustic measurements agrees well with the pH meter. Additionally, from figure 2, the standard deviation is higher at pH less than 7 because SNARF-5F absorbance is proportional to pH. At pH lesser than 7, the signal to noise ratio is lower which increases the standard deviation of the measured pH.

3.3 pH imaging in phantoms

After pH sensing experiments in tube phantoms, the next goal was to use the two microscopy systems (OR- and AR-PAM) to image pH distributions in tissue phantoms. The tube phantom was used for OR-PAM imaging experiments, and the well phantom was used for AR-PAM imaging.

Figure 3 shows the representative photoacoustic images obtained by scanning the phantoms with the OR- and AR-PAM systems. Figures 3A and 3B are the photoacoustic images obtained with OR-PAM at 565 and 580 nm optical wavelengths respectively. Similarly, figure 3C and 3D show the photoacoustic images obtained with AR-PAM at 565 and 580 nm optical wavelengths respectively.

For both OR- and AR-PAM, the two wavelength photoacoustic images were segmented by a mask matching the physical dimensions of the tubes and the wells. Next the relative concentrations of the acid and base forms of SNARF-5F were determined on pixel by pixel bases within the area of interest within the masked regions. Then the ratio of the relative concentrations was used to determine the pH at each pixel.

The same experiment was repeated with the addition of tissue. For OR-PAM, a 200 μm freshly excised mouse skin tissue was overlaid on the tube phantom. For AR-PAM, approximately 2 mm thick chicken breast tissue was overlaid on the well phantom. The overlaid tissue simulated the *in vivo* optical properties. Then the same process was repeated to determine the pH as mentioned above and the mean and standard deviations were compared with and without tissue overlay. Addition of tissue impacted the signal-to-noise ratio which increased the standard deviations of the measured pH with photoacoustic microscopy.

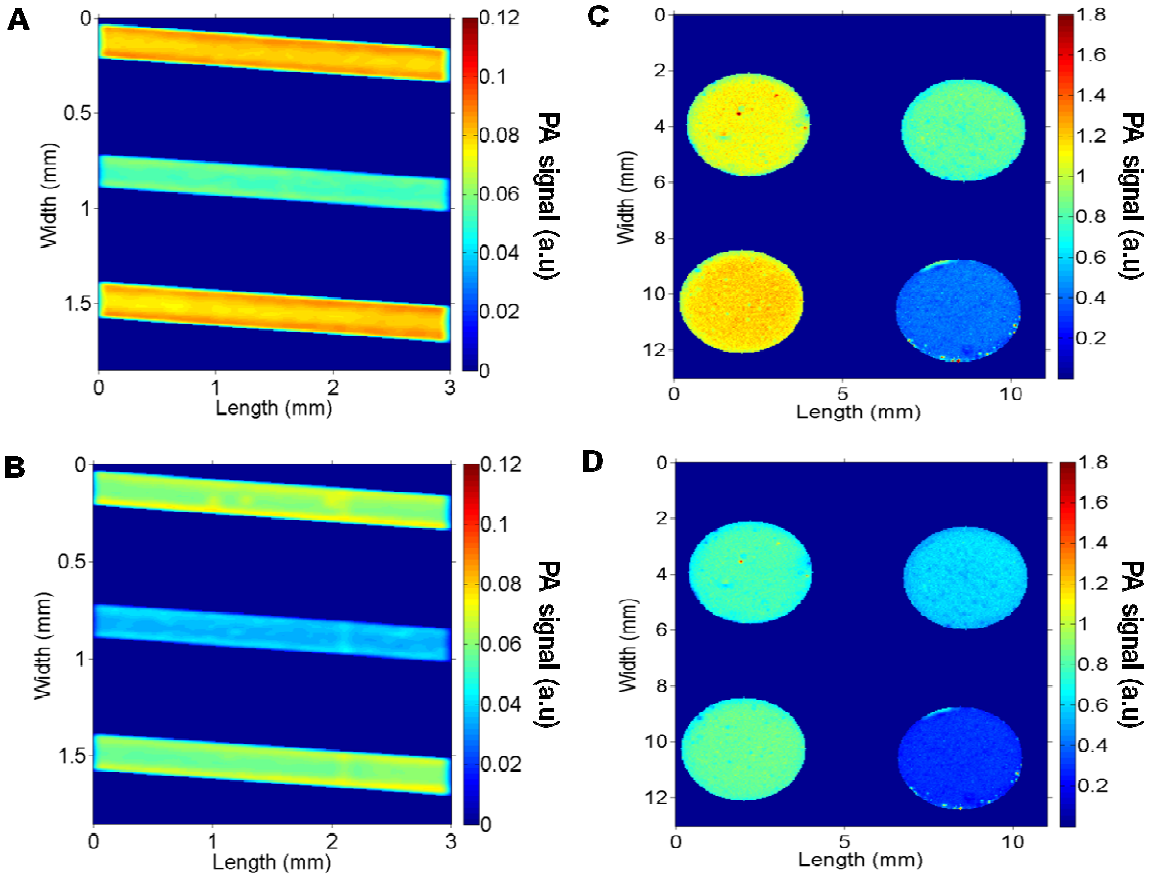

Figure 3. (A) Photoacoustic image of the tube pH phantom using OR-PAM at 565 nm, (B) 580 nm, (C) Photoacoustic image of well phantom using AR-PAM at 565 nm, (D) 580 nm optical wavelength.

4. CONCLUSIONS

pH imaging is possible using two wavelength photoacoustic microscopy up to a depth of 2 mm in biological tissue. Using two optical wavelengths, and linear least squares based spectral unmixing it is possible to recover pH values which are in close agreement with that measured from a commercial pH meter.

ACKNOWLEDGEMENTS

This work was supported in part by National Institutes of Health grants U54CA136398 and R01 EB000712. L. V. Wang has a financial interest in Microphotoacoustics, Inc and Endra, Inc, which, however, did not support this work.

[1] Porth, C. M., [Essentials of Pathophysiology], Lippincott Williams & Wilkins, USA, 159-208 (2010).
[2] Helmchen, F. and Denk, W., "Deep-tissue two-photon microscopy," Nature Methods 2(12), 932-940 (2005).
[3] Schlageter, B., Portling, S., Strauberger, J., Moreno-Bondi, M. C., Braslavsky, S.E. et al., "Development of an optoacoustic sensor module for pH and/or CO_2 determination aqueous solutions," Sensors and Actuators B 38-39, 3, 443-447 (1997).
[4] Maslov, K., Stoica, G. and Wang, L.V., "In vivo dark-field reflection mode photoacoustic microscopy," Optics Letters 30(6), 625-727 (2005).

[5] Zhang, H.F., Maslov, K., Stoica, G. and Wang, L.V., "Functional photoacoustic microscopy for high-resolution in vivo imaging,"
[6] Wang, L.V., "Multiscale photoacoustic microscopy and computed tomography" Nature Photonics 3(9), 503-509 (2009).
[7] Maslov, K., Zhang, H.F., Hu, S. and Wang, L.V., "Optical-resolution photoacoustic microscopy for in vivo imaging of single capillaries," Optics Letters 33(9), 929-931 (2008).